Isoelectronic perturbations to *f*-*d*-electron hybridization and the enhancement of hidden order in URu_2Si_2

Christian T. Wolowiec[a,b], Noravee Kanchanavatee[a,b,1], Kevin Huang[a,b,2], Sheng Ran[a,b,3], Alexander J. Breindel[a,b], Naveen Pouse[a,b,4], Kalyan Sasmal[a,b], Ryan E. Baumbach[c,d], Greta Chappell[c,d], Peter S. Riseborough[e], and M. Brian Maple[a,b,5]

[a]Department of Physics, University of California San Diego, La Jolla, CA 92093; [b]Center for Advanced Nanoscience, University of California San Diego, La Jolla, CA 92093; [c]National High Magnetic Field Laboratory, Florida State University, Tallahassee, FL 32310; [d]Department of Physics, Florida State University, Tallahassee, FL 32306; and [e]Physics Department, Temple University, Philadelphia, PA 19122

Contributed by M. Brian Maple, April 2, 2021 (sent for review December 27, 2020; reviewed by Sergey L. Bud'ko and Liling Sun)

Electrical resistivity measurements were performed on single crystals of $URu_{2-x}Os_xSi_2$ up to $x = 0.28$ under hydrostatic pressure up to $P = 2$ GPa. As the Os concentration, x, is increased, 1) the lattice expands, creating an effective negative chemical pressure $P_{ch}(x)$; 2) the hidden-order (HO) phase is enhanced and the system is driven toward a large-moment antiferromagnetic (LMAFM) phase; and 3) less external pressure P_c is required to induce the HO→LMAFM phase transition. We compare the behavior of the $T(x, P)$ phase boundary reported here for the $URu_{2-x}Os_xSi_2$ system with previous reports of enhanced HO in URu_2Si_2 upon tuning with P or similarly in $URu_{2-x}Fe_xSi_2$ upon tuning with positive $P_{ch}(x)$. It is noteworthy that pressure, Fe substitution, and Os substitution are the only known perturbations that enhance the HO phase and induce the first-order transition to the LMAFM phase in URu_2Si_2. We present a scenario in which the application of pressure or the isoelectronic substitution of Fe and Os ions for Ru results in an increase in the hybridization of the U-5*f*-electron and transition metal *d*-electron states which leads to electronic instability in the paramagnetic phase and the concurrent formation of HO (and LMAFM) in URu_2Si_2. Calculations in the tight-binding approximation are included to determine the strength of hybridization between the U-5*f*-electron states and the *d*-electron states of Ru and its isoelectronic Fe and Os substituents in URu_2Si_2.

hidden order | URu_2Si_2 | hybridization | pressure | isoelectronic

The heavy-fermion superconducting compound URu_2Si_2 is known for its second-order phase transition into the so-called "hidden-order" (HO) phase at a transition temperature $T_0 \approx 17.5$ K. Extensive investigation of the phase space in proximity to the HO phase transition has provided a detailed picture of the electronic and magnetic structure of this unique phase (1–42). However, more than three decades after the initial characterization of URu_2Si_2 (1–3), the order parameter for the HO phase is still unidentified.

Most perturbations to the URu_2Si_2 compound have the effect of suppressing HO. The application of an external magnetic field (H) suppresses the HO phase (41, 43) and many of the chemical substitutions (x) at the U, Ru, or Si sites that have been explored significantly reduce T_0, even at modest levels of substituent concentration (44–52). At present, only three perturbations are known to consistently enhance the HO phase in URu_2Si_2: 1) external pressure P, 2) isoelectronic substitution of Fe ions for Ru, and 3) isoelectronic substitution of Os ions for Ru. Upon applying pressure P, the HO phase in pure URu_2Si_2 is enhanced (6) and the system is driven toward a large-moment antiferromagnetic (LMAFM) phase (53). The HO→LMAFM phase transition is identified indirectly by a characteristic "kink" at a critical pressure $P_c \approx 1.5$ GPa in the T_0 (P) phase boundary (18, 53, 54) and also directly by neutron diffraction experiments, which reveal an increase in the magnetic moment from $\mu \sim (0.03 \pm 0.02)\mu_B$/U in the HO phase to $\mu \sim 0.4\ \mu_B$/U in the LMAFM phase (13, 55, 56).

Recent reports indicate that the isoelectronic substitution of Fe ions for Ru in URu_2Si_2 replicates the $T_0(P)$ behavior in URu_2Si_2 (57–59). An increase in x in $URu_{2-x}Fe_xSi_2$ enhances the HO phase and drives the system toward the HO→LMAFM phase transition at a critical Fe concentration $x_c \approx 0.15$ (58, 60). The decrease in the volume of the unit cell due to substitution of smaller Fe ions for Ru may be interpreted as a chemical pressure, P_{ch}, where the Fe concentration x can be converted to P_{ch} (x) (57, 59). In addition, the induced HO→LMAFM phase transition in $URu_{2-x}Fe_xSi_2$ occurs at combinations of x and P that consistently obey the additive relationship: $P_{ch}(x) + P_c \approx 1.5$ GPa (57, 59). These results have led to the

Significance

Phase transitions often manifest themselves in characteristic signatures in the electrical resistivity. Here, we track the temperature increase of the resistive signature of the hidden-order (HO) phase transition in URu_2Si_2, a mysterious phase with unknown order parameter. The application of pressure and the isoelectronic substitutions of Fe and Os ions for Ru are the only known perturbations to favor the HO phase. These perturbations are likely to cause increases in *f*-*d*-electron hybridization that lead to degeneracy and instabilities in the electronic band structure. The degeneracy is lifted by partial gapping of electronic states over the Fermi surface during the transition to HO. This and related investigations point to the importance of isoelectronic perturbations in generating emergent electronic phases.

Author contributions: C.T.W. and M.B.M. designed research; C.T.W., N.K., K.H., S.R., A.J.B., N.P., K.S., R.E.B., G.C., P.S.R., and M.B.M. performed research; C.T.W., P.S.R., and M.B.M. analyzed data; R.E.B. and G.C. performed EDX measurements; P.S.R. performed theoretical calculations; and C.T.W. and M.B.M. wrote the paper.

Reviewers: S.L.B., Ames Laboratory; and L.S., Institute of Physics.

The authors declare no competing interest.

[1]Present address: Department of Physics, Chulalongkorn University, Pathumwan 10330, Thailand.

[2]Present address: Materials Science Division, Lawrence Livermore National Laboratory, Livermore, CA 94550.

[3]Present address: Department of Physics, Washington University in St. Louis, St. Louis, MO 63130.

[4]Present address: Strategic Space Systems Division, Northrop Grumman, Redondo Beach, CA 90278.

[5]To whom correspondence may be addressed. Email: mbmaple@ucsd.edu.

This article contains supporting information online at https://www.pnas.org/lookup/suppl/doi:10.1073/pnas.2026591118/-/DCSupplemental.

Published May 11, 2021.

PHYSICS

suggestion that P_{ch} is equivalent to P in affecting the HO and LMAFM phases (58, 59).

Reports of the isoelectronic substitution of larger Os ions for Ru have shown that an increase in x in $URu_{2-x}Os_xSi_2$ 1) expands the volume of the unit cell, thus creating an effective negative chemical pressure ($P_{ch} \leq 0$); 2) enhances the HO phase; and 3) drives the system toward a similar HO→LMAFM phase transition at a critical Os concentration of $x_c \approx 0.065$ (60–62). These results are contrary to the expectation that a negative P_{ch} would lead to a suppression of HO and complicate the view of chemical pressure as a mechanism affecting the evolution of phases in URu_2Si_2.

In this paper, we report on the behavior of the $T(x, P)$ boundary for the $URu_{2-x}Os_xSi_2$ system based on $\rho(T)$ measurements of single crystals of $URu_{2-x}Os_xSi_2$ as a function of Os concentration x and applied pressure P. The $T(x, P)$ phase boundary observed here for the $URu_{2-x}Os_xSi_2$ system (57–59) is compared to that of the $URu_{2-x}Fe_xSi_2$ system and also with the behavior of $T(P)$ in pure URu_2Si_2. As an explanation for the enhancement of HO toward the HO→LMAFM phase transition, we suggest a scenario in which each of the perturbations of Os substitution, Fe substitution, and pressure P favors delocalization of the $5f$ electrons and increases the hybridization of the uranium $5f$-electron and transition metal (Fe, Ru, Os) d-electron states. To avoid an ad hoc explanation of the effect of increasing the Os concentration x in $URu_{2-x}Os_xSi_2$, compared to the effects of pressure P and Fe substitution, we explain how pressure P, Fe substitution, and Os substitution are three perturbative routes to enhancement of the U-$5f$- and d-electron hybridization. The importance of the $5f$- and d-electron hybridization to the emergence of HO/LMAFM is presented in the context of the Fermi surface (FS) instability that leads to a reconstruction and partial gapping of the FS during the transition from the paramagnetic (PM) phase to the HO and LMAFM phases (2, 6, 20, 22, 24–26, 37, 38, 63).

In an effort to further understand the effect of isoelectronic substitution on the $5f$- and d-electron hybridization, calculations in the tight-binding approximation were made for compounds from the series UM_2Si_2 (M = Fe, Ru, and Os). The calculations indicate that the degree of hybridization is largely dependent on the magnitude of the difference between the binding energy of the localized U-$5f$ electrons and that of the transition metal d electrons.

Results

Fig. 1 displays the temperature dependence of the ambient pressure electrical resistivity $\rho(T)$ in the vicinity of the transition temperature T_0 for the $URu_{2-x}Os_xSi_2$ system. The transition from the PM phase to the HO phase (or LMAFM phase at higher values of x) is defined to be at the location of the minimum in $\rho(T)$, which occurs prior to the upturn in $\rho(T)$ upon cooling, as indicated by the black arrow. It is clear that the feature in $\rho(T)$ shifts to higher temperature as x is increased.

The transition temperatures T_0, as determined from the $\rho(T)$ data shown in Fig. 1, were used to construct the T–x phase diagram displayed in Fig. 2. The values of T_0 are 17.1, 17.7, 17.8, 18.7, 19.9, 21.1, and 25.4 K for the single-crystal samples with x = 0, 0.07, 0.08, 0.15, 0.16, 0.18, and 0.28, respectively. The solid black lines that outline the $T_0(x)$ phase boundary between the PM phase and the HO (or LMAFM) phase are linear fits to the $T_0(x)$ data derived from the measurements reported herein. The solid black line of smaller slope outlining the $T_0(x)$ phase boundary between the PM phase and the HO phase is a linear fit to the $T_0(x)$ data for samples with low Os concentrations up to x = 0.15. The solid black line of larger slope outlining the $T_0(x)$ phase boundary between the PM phase and the LMAFM phase is a linear fit to the $T_0(x)$ data for the single-crystal samples with

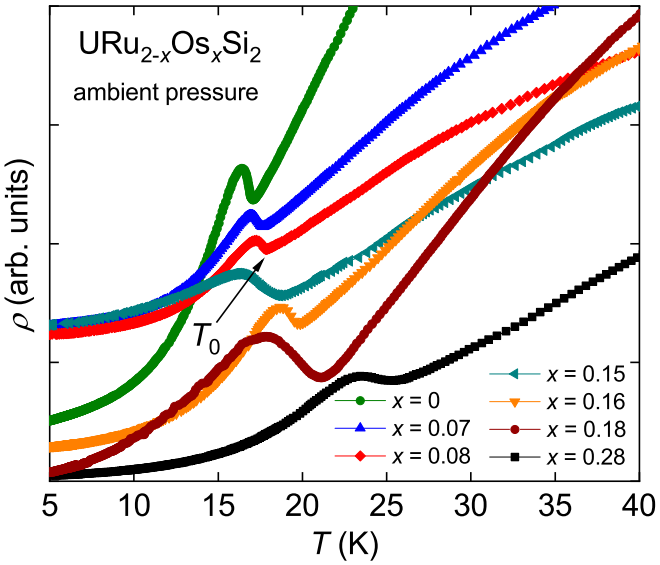

Fig. 1. Electrical resistivity $\rho(T)$ in the vicinity of the HO/LMAFM transition for the $URu_{2-x}Os_xSi_2$ system at ambient pressure for x = 0, 0.07, 0.08, 0.15, 0.16, 0.18, and 0.28. The transition temperature T_0 is indicated by the black arrow. The $\rho(T)$ curves have been shifted vertically for clarity.

Os concentrations from x = 0.15 to 0.28. The intersection of the two lines forms a kink in the $T_0(x)$ phase boundary and is taken to be the location of the HO→LMAFM transition at a critical Os concentration of $x_c \approx 0.14$. Included in the T–x phase diagram displayed in Fig. 2 are $T_0(x)$ data (white symbols) from previous reports. [These values of T_0 were determined from $\rho(T)$ measurements of polycrystalline samples (45, 61), from susceptibility $\chi(T)$ and muon spin resonance (μSR) measurements of single crystals (60), and from optical conductivity measurements of single crystals (62).] There is an obvious spread in the values of the $T_0(x)$ data, where the range of T_0 values is narrow at low concentrations of Os and diverges with increasing Os concentration for $x > 0.1$. A discussion of the variation in the $T_0(x)$ data as it relates to sample inhomogeneity and synthesis is included in *SI Appendix*.

Fig. 3 displays the temperature dependence of the electrical resistivity $\rho(T)$ near T_0 for the $URu_{2-x}Os_xSi_2$ system under applied pressure P. Fig. 3*A* displays $\rho(T)$ for pure URu_2Si_2 as a function of pressure up to $P \approx 1.9$ GPa. As pressure is increased, the feature in $\rho(T)$ shifts to higher temperature similar to what is observed with an increase in x. Furthermore, the feature in $\rho(T)$ appears to migrate more quickly with pressure above some critical pressure near 1.4 GPa. Fig. 3 *B* and *C* displays $\rho(T)$ in the vicinity of T_0 as a function of applied pressure for samples at x = 0.07 and 0.16, respectively. The sample with x = 0.07 (Fig. 3*B*) is at an Os concentration well below the critical concentration $x_c \approx 0.14$ and therefore exhibits the HO phase up to some critical pressure. As with the pure compound URu_2Si_2, the pressure dependence of the feature in $\rho(T)$ increases above some critical pressure P_c near 0.8 GPa. In contrast, for the sample with an Os concentration x = 0.16 greater than x_c, the pressure dependence of the feature in $\rho(T)$ is constant up to 2 GPa, suggesting the sample is likely already homogenous in the LMAFM phase at ambient pressure.

The $T_0(P)$ behavior for all seven single-crystal samples from the $URu_{2-x}Os_xSi_2$ system (at x = 0, 0.07, 0.08, 0.15, 0.16, 0.18, and 0.28) is plotted in the composite T_0 vs. P phase diagram shown in Fig. 4. The $T_0(P)$ phase boundaries for samples with x = 0, 0.07, and 0.08 exhibit the characteristic discontinuity or kink, which is indicative of the first-order HO→LMAFM phase transition. The slopes of the $T_0(P)$ phase boundaries in

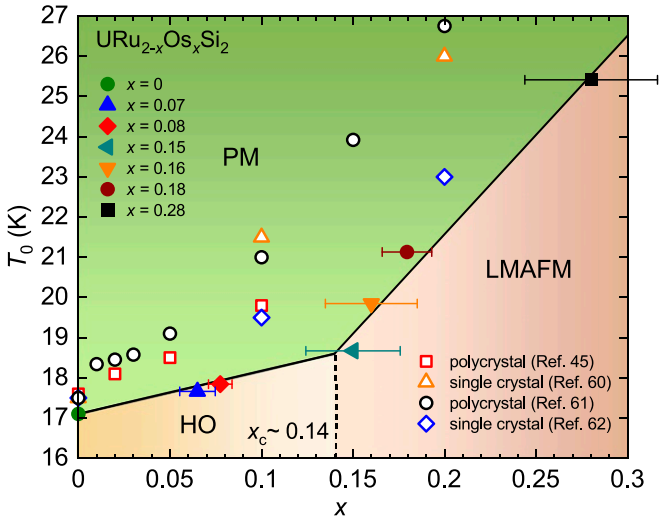

Fig. 2. A T_0 vs. x phase diagram for $URu_{2-x}Os_xSi_2$ up to $x = 0.28$. The values of the PM→HO/LMAFM transition temperature T_0 reported in this work (solid symbols) were determined from the $\rho(T)$ data displayed in Fig. 1 as explained in the main text. Additional values of T_0 (white symbols) from previous reports (45, 60–62) are included for comparison. The solid black lines representing the $T_0(x)$ phase boundaries are linear fits to the values of T_0. The vertical dashed line locates the critical Os concentration $x_c \approx 0.14$ at the HO→LMAFM phase transition. Error bars for x represent standard deviations in the data obtained from EDX measurements (*SI Appendix*).

the HO phase, prior to the discontinuities, for the $x = 0$, 0.07, and 0.08 samples are $dT_0/dP = 1.11$, 0.99, and 1.21 K·GPa^{-1}, respectively. In the LMAFM phase, the slopes are significantly higher at $dT_0/dP = 2.99$, 2.53, and 2.66 K·GPa^{-1}, respectively. There is no discontinuity in the slope of the $T_0(P)$ phase boundaries for the Os-substituted samples with higher Os concentrations of $x = 0.15$, 0.16, 0.18, and 0.28 that are above x_c, where the slopes were determined to be $dT_0/dP = 2.31$, 2.42, 2.15, and 2.27 K·GPa^{-1}, respectively. Note the equivalence between the values of the pressure dependence in both the HO phase (averaged at $dT_0/dP \approx 1.10$ K·GPa^{-1}) and the LMAFM phase (averaged at $dT_0/dP = 2.47$ K·GPa^{-1}) across all of the samples. The values of all slopes were determined by linear fits (solid lines in Fig. 4) to the $T_0(P)$ data in the HO or LMAFM phases and are in very good agreement with hydrostatic pressure coefficients reported in other investigations (18, 53, 59, 64).

The pressure dependence of the charge gap Δ that opens up over the Fermi surface during its reconstruction at the PM→HO/LMAFM phase transition may serve as another measure of the critical pressure P_c. Namely, the critical pressure P_c can be taken as the value of P where there is a change in the pressure dependence of the charge gap ($d\Delta/dP$) that occurs at the first-order phase transition from HO to LMAFM. Fig. 5 displays a plot of the charge gap Δ as a function of pressure P for single-crystal samples of $URu_{2-x}Os_xSi_2$ with $x = 0$, 0.07, 0.08. The values of Δ were extracted from fits of a theoretical model of electrical resistivity (65) to the low-temperature $\rho(T)$ data below the HO transition as described in ref. 59. There is a flattening of the pressure dependence (or slope $d\Delta/dP$) in the $\Delta(P)$ curves for the $x = 0$, 0.07, 0.08 samples at pressures $P \approx 1.55$, 0.90, and 0.50 GPa, respectively. These are consistent with the critical pressures $P_c = 1.43$, 0.75, 0.33 GPa determined from the $T_0(P)$ phase boundaries in Fig. 4. The saturation of $\Delta(P)$ indicates the full transition into the LMAFM phase and there is a consistent ~0.15 GPa lag in the location of the kinks in $\Delta(P)$ relative to the respective values of P_c. The regions with large $d\Delta/dP$ just prior to the kinks in $\Delta(P)$ are indicative of a percolation of the LMAFM phase with increasing pressure. This percolation of the LMAFM phase begins at $P = 0.75$ GPa for $x = 0$, almost immediately at $P = 0.2$ GPa for $x = 0.07$, and immediately at $P = 0$ GPa for $x = 0.08$. Hence, while low values of $\Delta \approx 7.0$ meV

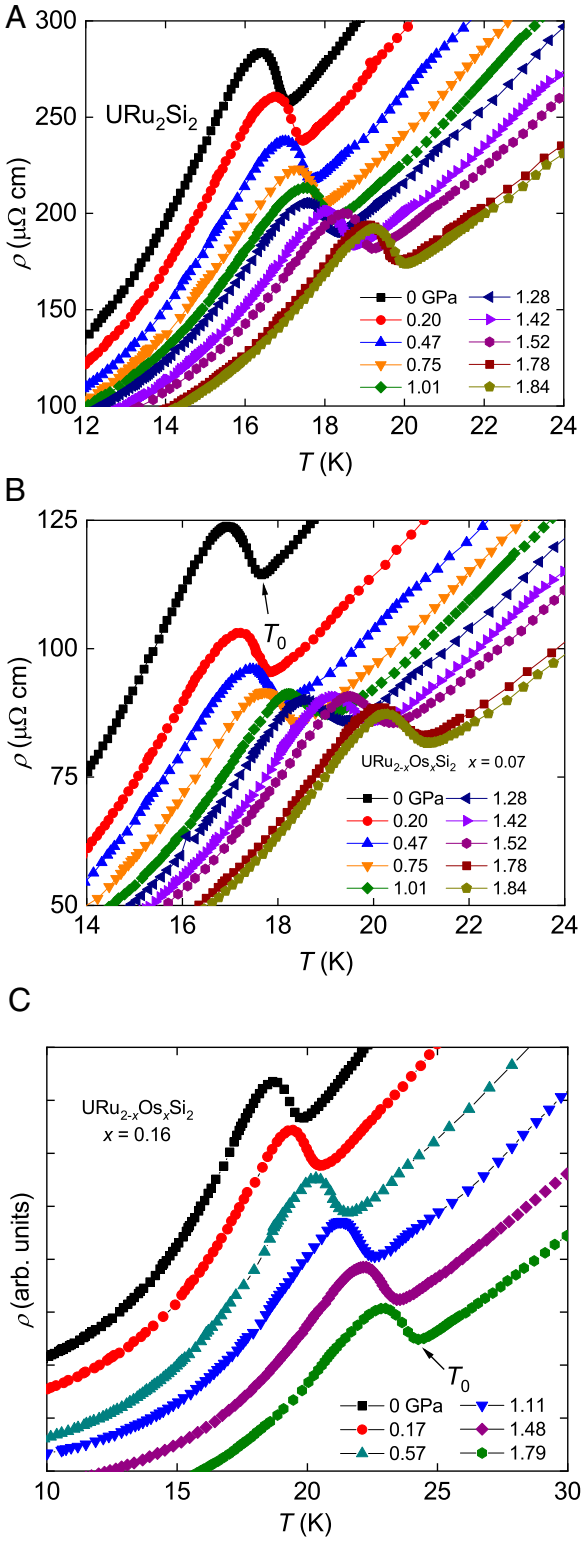

Fig. 3. Electrical resistivity $\rho(T)$ in the vicinity of the HO/LMAFM transition for the $URu_{2-x}Os_xSi_2$ system as a function of pressure P: (*A*) $\rho(T)$ for pure URu_2Si_2 as a function of pressure up to $P = 1.9$ GPa, (*B*) $\rho(T)$ for the $x = 0.07$ sample as a function of pressure up to $P = 1.9$ GPa, and (*C*) $\rho(T)$ for the $x = 0.16$ sample as a function of pressure up to 1.8 GPa. The $\rho(T)$ data for $x = 0.16$ have been shifted vertically for clarity.

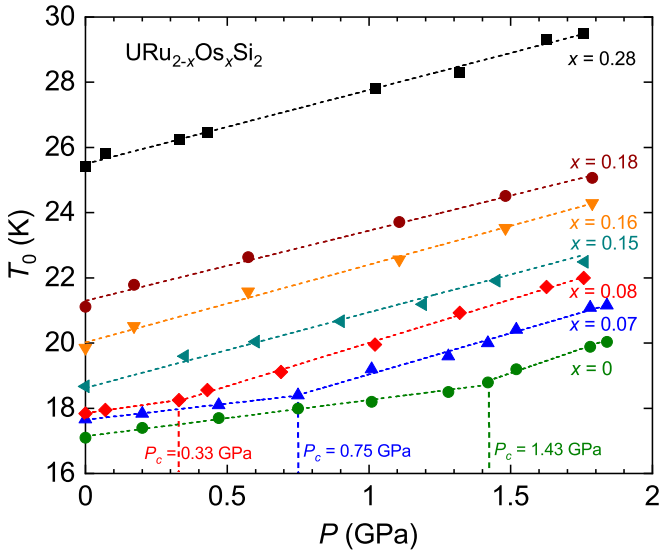

Fig. 4. A composite T_0 vs. P phase diagram for $URu_{2-x}Os_xSi_2$. The dashed lines representing the $T_0(P)$ phase boundary are linear fits to the $T_0(P)$ data. The values of the critical pressures P_c = 1.43, 0.75, and 0.33 for x = 0, 0.07, and 0.08, respectively, mark the pressure-induced HO→LMAFM phase transition and are defined by the location of the kinks in the $T_0(P)$ phase boundaries (or intersections of the linear fits) (see main text).

correspond to transitions into the HO phase, higher values of $\Delta > 8.5$ meV correspond to transitions into the LMAFM phase. Intermediate values of Δ that precede the flattening of Δ (P) are indicative of a mixture of HO and LMAFM phases, with an increase in the fraction of the LMAFM phase occurring as pressure is increased.

Of central importance to the current report is the reduction of the critical pressure P_c with increasing Os concentration x, as illustrated in Fig. 4. The vertical dashed lines locate decreasing values of P_c = 1.43, 0.75, and 0.33 GPa for samples in order of increasing Os concentration x = 0, 0.07, and 0.08. This is reminiscent of the reduction of P_c with increasing Fe concentration for the $URu_{2-x}Fe_xSi_2$ system (59). Based on the results of the Fe-substituted system, in which lower values of P_c were required to induce the HO→LMAFM transition according to the additive relation $P_{ch}(x) + P_c \approx 1.5$ GPa, one would expect that higher (rather than lower) values of P_c are required to induce the HO→LMAFM transition for Os-substituted URu_2Si_2, which is biased with an effective negative chemical pressure ($P_{ch}(x) < 0$). However, this is not what we observed.

The discrepancy between the expected increase in P_c and the reduction in P_c that was observed experimentally is illustrated in the plot of P_c vs. x as shown in Fig. 6. The solid black line with a negative slope is a linear fit to the experimentally determined values of P_c (solid symbols) and represents the $P_c(x)$ phase boundary between the HO and LMAFM phases for the $URu_{2-x}Os_xSi_2$ system. The extrapolation of the fit to zero pressure yields a critical Os concentration of x = 0.12, which is comparable to the value of x_c = 0.14 determined from the kink in the $T_0(x)$ phase boundary displayed in Fig. 2. The open symbols in Fig. 6 represent the expected values of critical pressure P_c, which were determined by first converting the Os concentration x to a negative chemical pressure $P_{ch}(x)$ and then using the additive property of chemical and applied pressure: $P_{ch}(x) + P_c \approx 1.5$ GPa. The solid red line with positive slope is a linear fit to these expected values of P_c and represents the expected $P_c(x)$ phase boundary between the HO and LMAFM phases for the $URu_{2-x}Os_xSi_2$ system.

Other than pure URu_2Si_2, Fe-substituted URu_2Si_2, and Os-substituted URu_2Si_2, the only known URu_2Si_2-based system containing transition metal solutes measured under pressure is Re-substituted URu_2Si_2 (18). At ambient pressure, the effect of Re substitution is to rapidly suppress HO toward an emergent itinerant ferromagnetic phase. Interestingly, as pressure is applied to samples from the $URu_{2-x}Re_xSi_2$ system, the HO phase is enhanced toward the same HO→LMAFM phase transition. However, as the Re concentration is increased in $URu_{2-x}Re_xSi_2$ under pressure, the kink in the T_0 vs. P composite phase diagram persists at a critical pressure of P_c = 1.5 GPa. This difference is emphasized in Fig. 7, which displays T_0–P–x phase diagrams for each of the $URu_{2-x}Os_xSi_2$, $URu_{2-x}Fe_xSi_2$, and $URu_{2-x}Re_xSi_2$ systems. The $T_0(x, P)$ data for the $URu_{2-x}Re_xSi_2$ system were taken from ref. 18. (Due to the fact that the HO transition temperature T_0 is suppressed with increasing Re concentration, the values along the concentration $[x]$ axis in Fig. 7*C* have been reversed for clarity.) Note the difference in the HO/LMAFM phase boundary in the x–P plane for the Re-substituted system in Fig. 7*C*. The HO/LMAFM phase boundary is constant at P_c = 1.5 GPa for all Re concentrations up to x = 0.08 in $URu_{2-x}Re_xSi_2$, while the boundary is suppressed to P = 0 GPa as x is increased in the $URu_{2-x}Fe_xSi_2$ and $URu_{2-x}Os_xSi_2$ systems.

Discussion

Investigations of URu_2Si_2 under applied uniaxial and/or hydrostatic pressure show that an increase in pressure enhances HO (with an increase in T_0) and drives the system toward a pressure-induced antiferromagnetic phase (LMAFM) at a critical pressure of $P_c \approx 1.5$ GPa at the bicritical point (or at $P_x \approx 0.5$ GPa as $T \rightarrow 0$) (13, 18, 53, 64, 66–71). Recently, a related investigation of Fe-substituted URu_2Si_2 under applied pressure established a quantitative equivalence between positive chemical pressure $P_{ch}(x)$ and external pressure P in affecting the formation of electronic phases in URu_2Si_2 (59). The equivalence between $P_{ch}(x)$ and P is reflected in the consistent additive relationship $P_{ch}(x) + P_c \approx 1.5$ GPa, where the critical pressure P_c necessary to drive the HO→LMAFM phase transition in $URu_{2-x}Fe_xSi_2$

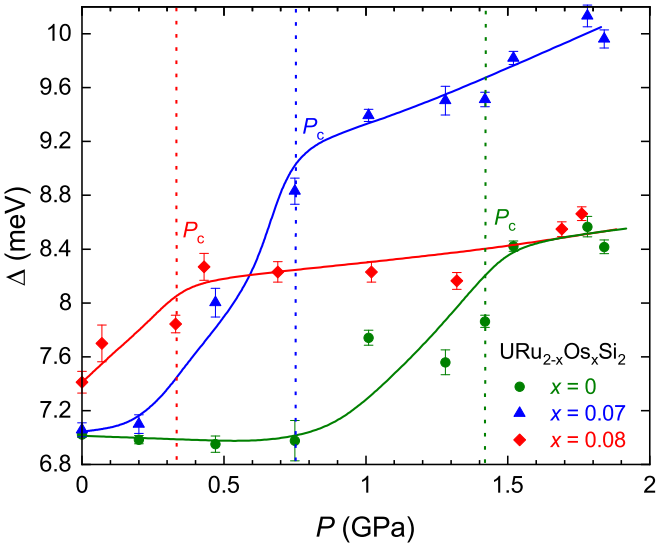

Fig. 5. Energy gap Δ vs. pressure P for the x = 0, 0.07, and 0.08 samples. The values of Δ are based on fits to the low-temperature $\rho(T)$ data as explained in the main text. The values of P_c (marked by dashed vertical lines) were determined from the kinks in the $T_0(P)$ phase boundaries in the T_0 vs. P phase diagram displayed in Fig. 4. The error in Δ was determined by the fitting algorithm and the solid lines are guides to the eye.

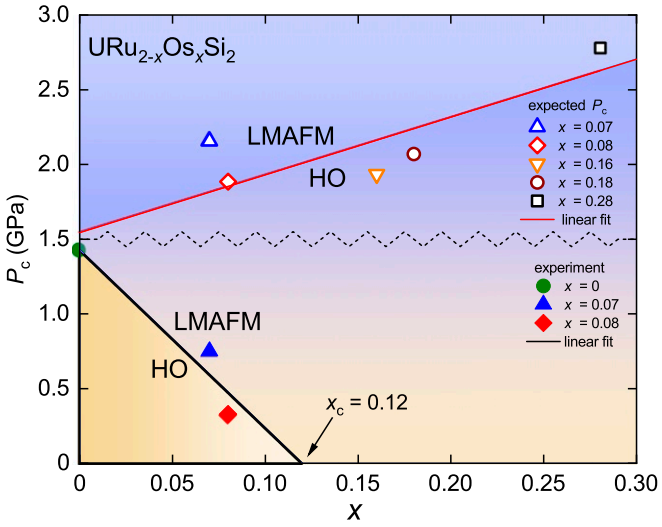

Fig. 6. Measured and expected critical pressure P_c as a function of x for $URu_{2-x}Os_xSi_2$. As x is increased, the critical pressure is reduced to P_c = 0 GPa at a critical Os concentration of $x_c \sim 0.12$. The open symbols represent the expected critical pressure P_c (see main text). The black (red) solid lines represent the experimental (expected) HO/LMAFM phase boundaries and are linear fits to the experimental (expected) values of critical pressure P_c.

decreases with increasing Fe concentration x. The relevance of pressure- and chemical substitution-induced changes to the lattice and how they relate to hybridization between f- and d-electron states are discussed in more detail below.

The results presented here for the effect of increasing Os concentration x on the enhancement of HO in $URu_{2-x}Os_xSi_2$, as well as the reduction of the critical pressure P_c that induces the HO→LMAFM transition, are remarkably similar to the behavior reported for Fe-substituted URu_2Si_2 (59). However, the isoelectronic substitutions of Fe and Os have contrasting effects on the body-centered-tetragonal (bct) lattice. Substitution of smaller Fe ions at the Ru site leads to a contracted lattice and a positive chemical pressure $P_{ch}(x)$ in $URu_{2-x}Fe_xSi_2$, while substitution of larger Os ions at the Ru site leads to an expanded lattice and a negative chemical pressure $P_{ch}(x)$ in $URu_{2-x}Os_xSi_2$ (The effect of Os substitution on the lattice is discussed in *SI Appendix*.) This complicates the view of a reduction in the unit-cell volume through applied or chemical pressure as a necessary condition for the enhancement of HO in URu_2Si_2.

Here we suggest an increase in the hybridization of the uranium 5f-electron states and transition metal d-electron states as the cause for the enhancement of HO toward the HO→LMAFM phase transition in URu_2Si_2. High-resolution angle-resolved photoemission spectroscopy (ARPES) and scanning-tunneling microscopy (STM) measurements show directly that the HO phase emerges from a PM Kondo-like phase that has clear signatures of hybridization between the localized 5f- and itinerant spd-electron states, with the onset of the correlated-electron heavy-fermion state near a coherence temperature $T_{coh} \approx 70$ K (22, 24–26, 37). At lower temperatures close to the HO transition temperature T_0, there is an increase in the 5f-d-electron hybridization leading to a FS instability as more U-5f electrons dissolve into the FS (22, 24–26, 36, 37, 72). The degenerate crossing of hybridized 5f-d bands at the Fermi energy E_F creates density-of-states "hot spots" or instabilities at the FS in the PM phase (20, 27). Hence, small perturbations to the electronic structure in the PM phase may lift the degeneracy and remove the FS instability, leading to the opening of an energy gap over roughly 70% of the FS in the HO and LMAFM phases and a rehybridization of the 5f- and d-electron states. Such a topological reconstruction of the FS is observed during the second-order symmetry-breaking transition (or Lifshitz transition) from the PM phase to the HO or LMAFM phases.

In this report, we suggest that when URu_2Si_2 is tuned with pressure or with either of the isoelectronic substitutions of Fe or Os at the Ru site, subtle changes occur to the 5f-d-electron hybridization near the Fermi level which favor the stability of the gapped FS of the HO (or LMAFM) phase over the instability of the FS in the Kondo-like PM phase. As a result, there is an observed increase in the transition temperature T_0 with increasing pressure P or substituent concentration x. This applies to the observed increase in T_N for the PM→LMAFM phase transition, during which the FS undergoes a similar reconstruction and gapping. Inelastic neutron scattering experiments performed on single crystals from the $URu_{2-x}Fe_xSi_2$ system reveal similar interband correlations where enhanced local-itinerant electron hybridization also leads to the stability of the LMAFM phase (73). Below, we address the manner in which each of the three perturbations (pressure, Fe substitution, and Os substitution) independently favors the hybridization of the U-5f- and d-electron states. Hence, the additivity of x and P in enhancing HO and inducing the LMAFM phase in both the $URu_{2-x}Fe_xSi_2$ and $URu_{2-x}Os_xSi_2$ systems can also be explained.

Pressure. Application of both uniaxial and hydrostatic pressure reveals that the pressure dependence of the HO transition temperature T_0 is anisotropic with respect to changes in the a and c lattice parameters of the tetragonal crystal. The a lattice parameter (or the shortest U-U separation in the basal plane of the tetragonal lattice) appears to be important in affecting the magnetic properties of URu_2Si_2, as well as the transition to the LMAFM phase (64, 70). Furthermore, it has been shown that it is not possible to induce the HO→LMAFM phase transition with uniaxial stress along the c axis (70). Nor does the ratio of lattice parameters c/a appear to be important in governing the salient magnetic properties of URu_2Si_2 and the formation of its extraordinary electronic phases (70). These pressure-induced changes in the lattice are closely connected to spatial and energetic changes that may occur to the s-, p-, d-, and f-electronic orbitals. It is well known that the application of pressure reduces the interatomic distance within a crystal lattice, leading to the delocalization and overlapping of electronic orbitals (74–77). As a consequence, applied pressure can lead to an increase in the hybridization between f- and d-electron states (78–80), which is important for the formation of the HO phase and is now considered to be one of its defining characteristics (22, 36, 72). Here, we suggest that the pressure-induced enhancement of hybridization in URu_2Si_2-based systems contributes to the instability at the FS that leads to the gapping of the FS and the second-order transition to the HO and LMAFM phases.

Fe Substitution. The remarkable agreement between $P_{ch}(x)$ and P and their effect on the HO and LMAFM phases is not a surprise, considering that Fe substitution results in a reduction of volume that is almost entirely associated with a decrease in the basal-plane lattice parameter a. Upon substitution of smaller Fe ions for Ru, it is suggested that the effective chemical pressure P_{ch} associated with the reduction in the interatomic spacing favors increased overlap and hybridization of the U-5f-electron and d-electron states in much the same way that applied pressure P favors hybridization (57, 59). Hence, the investigations of URu_2Si_2 under pressure and with Fe partially substituted for Ru suggest that a reduction of the basal-plane lattice parameter a is necessary for the enhancement of HO and the HO→LMAFM transition in URu_2Si_2 (57–59). In addition to the comparable

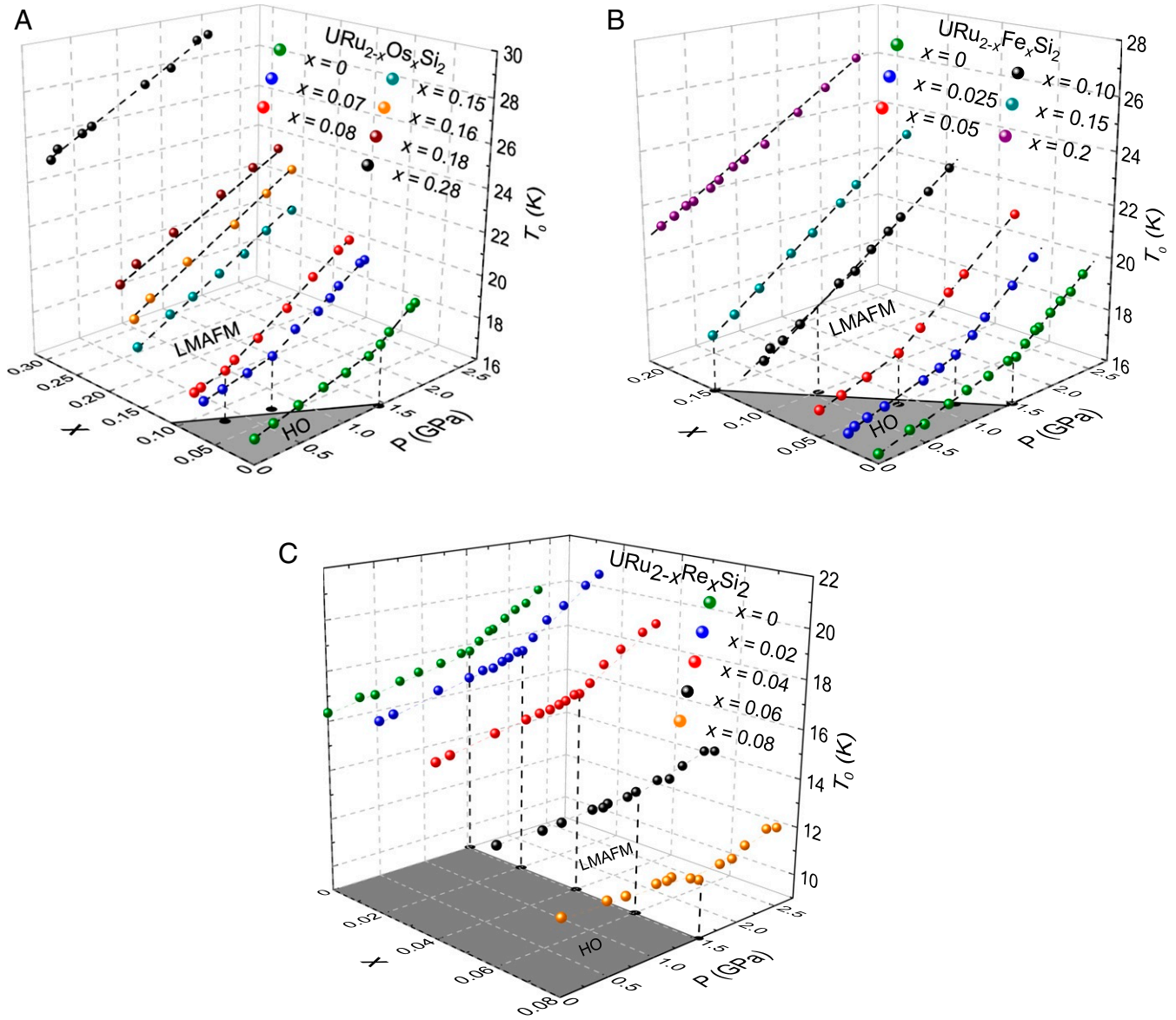

Fig. 7. (*A*–*C*) T_0–*P*–*x* phase diagrams for the (*A*) $URu_{2-x}Os_xSi_2$, (*B*) $URu_{2-x}Fe_xSi_2$, and (*C*) $URu_{2-x}Re_xSi_2$ systems. The values along the concentration (*x*) axis for the $URu_{2-x}Re_xSi_2$ system in *C* are reversed relative to those of *A* and *B*. The $T_0(x, P)$ data for the $URu_{2-x}Re_xSi_2$ system were taken from ref. 18.

effects of Fe substitution and pressure on the lattice, HO, and LMAFM, we discuss below the binding energy of the Fe-4d electrons as a relevant factor for the increase in 5f- and d-electron hybridization.

Os Substitution. In contrast, the effective negative chemical pressure associated with an expanded crystal lattice upon substitution of larger Os ions for Ru should not favor hybridization of the U-5f- and d-electron states in $URu_{2-x}Os_xSi_2$. However, an increase in the hybridization may still occur if one considers one or both of the following: 1) the larger spatial extent of the 5d-electron orbitals of osmium (with a radius of 0.706 Å) compared to that of the 4d-electron orbitals of ruthenium (with a radius of 0.639 Å) (81, 82). In the tight-binding approximation, the overlap of a pair of electronic orbitals is dominated by an exponential term which decays on a length scale given by the inverse sum of the radii of the two orbitals (83–85). The increase in the radius of the d-electron wave functions when an Os ion replaces a Ru ion is substantial and would significantly affect the overlap of the d-electron wave functions and U-5f-electron wave functions. 2) The stronger spin–orbit coupling that occurs in Os compared to that of Ru may lead to a broadening of the d-electron energy bands and an increase in the number of d electrons at the Fermi level (27).

Calculations of *f*- and *d*-Electron Hybridization in UM_2Si_2 with *M* = (Fe, Ru, and Os). In an effort to further understand the hybridization between the U-5f-electron and transition metal d-electron states in the UM_2Si_2 series with M = (Fe, Ru, and Os), we performed tight-binding calculations of the overlap of the U-5f-electron states and d-electron states of the Fe, Ru, and Os ions.

Table 1 contains the hybridization energies as a measure of the degree of hybridization between the U-5f-electron states and the d-electron states of Fe, Ru, and Os. The hybridization energies $\Delta_\alpha(R)$ are smallest for the hybridization of Ru d electrons, which suggests a diminished hybridization for the d electrons of the Ru ions compared to those of the Fe and Os ions.

Table 1. Hybridization energies of the αth 5*f* orbital with the βth *d* orbital, where the energies are given in Rydbergs (Ry)

$\Delta_\alpha(R)$	Fe (Ry)	Ru (Ry)	Os (Ry)
$\Delta_{xyz}(R)$	0.081	0.034	0.097
$\Delta_{x(5x^2-3r^2)}(R)$	0.058	0.025	0.064
$\Delta_{y(5y^2-3r^2)}(R)$	0.050	0.021	0.055
$\Delta_{z(5z^2-3r^2)}(R)$	0.079	0.033	0.087
$\Delta_{x(y^2-z^2)}(R)$	0.039	0.018	0.047
$\Delta_{y(z^2-x^2)}(R)$	0.039	0.018	0.047
$\Delta_{z(x^2-y^2)}(R)$	0.067	0.028	0.084

Hybridization of the Os d-electron states with the U-5f-electron states is largest, being only slightly larger than that of the Fe d-electron states. This ordering of $\Delta_\alpha(R)$ for Fe, Ru, and Os is attributed to both the increasing spatial extent of the d-electron wave function down the column of the periodic table (*SI Appendix*, Fig. S5) and the nonmonotonic variation in excitation energy (or binding energy). However, the nonmonotonic variation in binding energy is the dominant effect, where the binding energy of the Ru d electrons is much lower than that of the Fe and Os d electrons and also the f electrons of U (*SI Appendix*, Table S1).

Similar trends in 4f-d-electron hybridization are reported for the heavy-fermion and Kondo-like systems of $CeFe_2Si_2$, $CeRu_2Si_2$, and $CeRu_{2-x}Os_xSi_2$, where the strength of the hybridization of the Ce-4f electrons and the s, p, and d conduction electrons can be characterized by the Kondo temperature T_K (86). $CeFe_2Si_2$ has a large Kondo temperature $T_K \sim 103$ K (87), while T_K for $CeRu_2Si_2$ is ~10 to 25 K (86, 88–90). As small amounts of Os are introduced into $CeRu_{2-x}Os_xSi_2$, the Kondo temperature increases to $T_K \sim 10^2$ K for $x = 0.1$ (89, 91). These changes in the hybridization of the Ce-4f and s, p, and d electrons across the $CeFe_2Si_2$, $CeRu_2Si_2$, and $CeRu_{2-x}Os_xSi_2$ systems appear to be consistent with the changes in the 5f-d-electron hybridization in other reports (92) and with our calculations across the UM_2Si_2 series with M = Fe, Ru, and Os.

Hence, the enhancement of the HO phase in $URu_{2-x}Os_xSi_2$ with increasing Os concentration x is consistent with the greater degree of d- and f-electron hybridization as calculated for the Os ions. Similar reasoning may also explain the enhancement of HO in the case of URu_2Si_2 under applied pressure P and the case of $URu_{2-x}Fe_xSi_2$ with increasing Fe concentration x. The reduction of the critical pressure P_c and the cooperative effects of x and P observed in $URu_{2-x}Os_xSi_2$ may follow from the nature in which both the perturbations of x and P work together to foster hybridization: Applied pressure favors delocalization of the U-5f electrons and the substitution of Os ions for Ru extends the d electrons outward within the unit cell. Both of these effects together would favor overlap between the U-5f- and d-electron wave functions in $URu_{2-x}Os_xSi_2$.

The increase in spin–orbit coupling may also help with hybridization of the U-5f- and Os-5d-electron states on account of the splitting of the d-electron band, which brings the orbitals closer together in energy and slightly enhances the hybridization between the two orbital levels with $j = l - 1$, where $l = 3$ for U and $l = 2$ for Os. The increase in hybridization between the U-5f-electron and transition metal d-electron states, caused by the larger spin–orbit coupling of Os, is estimated to be limited and less than ~2% (85).

The persistence of the critical pressure at $P_c = 1.5$ GPa, with increasing rhenium (Re) concentration in $URu_{2-x}Re_xSi_2$, suggests that any doping which suppresses HO may not be additive with pressure and, as such, is not a perturbation that favors hybridization. Indeed, for small Re concentration ($x < 0.1$) in $URu_{2-x}Re_xSi_2$, the hidden-order transition temperature T_0 is rapidly reduced, and for higher Re concentrations ($x > 0.1$), the system enters a ferromagnetic state rather than the LMAFM phase. Based on our hybridization calculations and previous reports of the trends in 5f-d-electron hybridization for the 3d-, 4d-, and 5d-electron orbitals, one might expect the same qualitative increase in hybridization (relative to the Ru-4d electrons) for the Re-5d-electron states as observed for the Os-5d-electron states. However, the trends in 5f-d-electron hybridization reported here for UM_2Si_2 (M = Fe, Ru, and Os) and elsewhere for CeM_2Si_2 (M = Fe, Ru, and Os) (86, 88–91) are for systems that are isoelectronic. For these systems, there is little or no variation across the series in the number of d-band electrons near the Fermi energy E_F that are available for hybridization. The degree of f-d-electron hybridization is largely dependent on the density of states at the Fermi level such that any significant variation in the number of d electrons near E_F would have an effect on the hybridization (45, 92). Furthermore, nonisoelectronic substitutions for Ru with elements such as Rh and Re that are effectively electron (or hole) donors would shift the Fermi level away from the degenerate crossing of the hybridized bands, thereby stabilizing the FS in the paramagnetic phase. In addition, charge carrier doping associated with nonisoelectronic substituents might also change the underlying band structure and shape of the FS, which experimentally has been shown to suppress HO (93, 94).

Hence, there are competing effects on hybridization in moving from Ru to Re, where any increase in hybridization owing to the spatially extended character of Re-5d electrons is mitigated by the deleterious effect of the reduction in the number of d electrons available near E_F due to the substitution of Re ($5d^5$) for Ru ($4d^6$). In addition, the degree of hybridization between U-5f and Re-5d electrons depends not only on the hybridization matrix elements but also largely on the binding energy of the Re-5d electrons (*SI Appendix*, Eq. **1**). For systems in which the HO phase is suppressed with increasing substituent x, as in Re-substituted URu_2Si_2, a determination of the hybridization between the U-5f and Re-5d electrons as a function of concentration x should be investigated further.

Concluding Remarks

Early specific heat measurements of URu_2Si_2 in 1985 revealed an anomalous feature at $T_0 = 17.5$ K, reminiscent of a continuous mean-field type of phase transition (2). The use of a simple model for the analysis of the specific heat anomaly led to the notion of a partial gapping of the Fermi surface as the compound entered the HO phase, with the magnitude of the gap determined to be 11 meV (2). This simple yet powerful experimental technique was one of the first "probes" into the structure or reconstruction of the Fermi surface during the HO phase transition in URu_2Si_2. Over the last 20 y, advanced experimental techniques have yielded direct evidence and provided confirmation of the partial gapping of the Fermi surface, with gap values of ~10 meV. We now have a detailed picture of the electronic structure in proximity to the HO transition at T_0, whereby the onset of coherence near 70 K leads to a degenerate crossing of 5f-d-hybridized bands at the Fermi level and ultimately to an instability, partial gapping, and reconstruction of the Fermi surface at 17.5 K.

Currently, applied pressure and the substitution of Fe and Os ions for Ru are the only known perturbations to URu_2Si_2 that result in an enhancement of HO and a subsequent first-order transition to the LMAFM phase. Here, we explain the enhancement of HO as the result of an increase in the hybridization of the uranium 5f-electron and transition metal (Fe, Ru, Os) d-electron states, which leads to a Fermi surface instability that

PHYSICS

favors the HO phase over the PM phase. This causes the increase in the PM→HO transition temperature T_0.

The results from transport measurements for single crystals of $URu_{2-x}Os_xSi_2$ under pressure presented here are used to construct the T_0–P–x phase diagram. As the concentration of Os is increased, there are both an observed increase in T_0 and a reduction in the critical pressure P_c necessary to induce the transition to the LMAFM phase. This is consistent with previously reported effects of applied pressure and Fe substitution on HO and P_c in single crystals of $URu_{2-x}Fe_xSi_2$. However, substitution of Os in URu_2Si_2 leads to an expansion of the lattice, whereas application of pressure and introduction of Fe into URu_2Si_2 result in a contraction of the lattice.

Hence, the increase in the $5f$- and d-electron hybridization appears to be dependent on various effects, both spatial and energetic. The contraction of the lattice with pressure or chemical pressure tends to favor both the overlap and hybridization of electronic orbitals, whereas the spatially extended d-electron orbitals (as with Os-$5d$ electrons) can also lead to an increase in their hybridization with the localized $5f$ electrons. In this report, results of tight-binding calculations show that the degree of hybridization between the U-$5f$ electrons with the transition metal d electrons is largely dependent on the difference in binding energy between the localized $5f$ electrons and d-band electrons. In general, it is noted that the trend in hybridization increases in moving away from the Ru-$4d$ electrons to the Fe-$3d$ and Os-$5d$ electrons. This is also true for other isoelectronic systems such as CeM_2Si_2 (M = Fe, Ru, and Os).

Materials and Methods

Synthesis and Sample Quality. The experimental design and procedure, including synthesis of single crystals, crystallographic measurements, and measurements of electrical resistivity under applied pressure, are similar to those in the investigation of the $URu_{2-x}Fe_xSi_2$ system as described in ref. 59. Single crystals of $URu_{2-x}Os_xSi_2$ at nominal concentrations of x_{nom} = 0, 0.025, 0.05, 0.10, 0.13, 0.16, and 0.20 were grown according to the Czochralski method in a tetra-arc furnace. The quality of the single-crystal samples was assessed by Laue and powder diffraction measurements. The lattice parameters were determined from fits to the X-ray diffraction data according to the Rietveld refinement technique using the GSAS-II software package (95). Elemental analysis of single-crystal samples of $URu_{2-x}Os_xSi_2$ at nominal concentrations of x_{nom} = 0.025, 0.05, 0.10, 0.13, and 0.20 was performed using energy-dispersive X-ray spectroscopy (EDX). Based on the EDX measurements, the actual osmium concentrations x_{act} in these samples were determined to be x_{act} = 0.07, 0.08, 0.15, 0.18, and 0.28, respectively. In this report, the Os concentration x in the single-crystal $URu_{2-x}Os_xSi_2$ samples is taken as x_{act} as determined from the EDX measurements, unless otherwise stated. It is noted that the single-crystal sample with nominal Os concentration x_{nom} = 0.16 was not available for EDX measurement and thus x was taken as x_{nom} = 0.16 in this case. (See *SI Appendix* for details on sample quality and the variation in the Os concentration x within a sample.)

Electrical Resistivity. Electrical resistivity ρ (T) measurements were performed on single crystals of $URu_{2-x}Os_xSi_2$ under applied pressure up to P = 2 GPa for Os concentrations x = 0, 0.07, 0.08, 0.15, 0.16, 0.18, and 0.28. Annealed Pt wire leads were affixed with silver epoxy to gold-sputtered contact surfaces on each sample in a standard four-wire configuration so that the current is directed parallel to the *ab* plane (or basal plane). The single-crystal samples were naturally cleaved along the *ab* plane (or perpendicular to the *c* axis) after annealing and Laue X-ray diffraction patterns were used to confirm the orientation of the body-centered-tetragonal crystal structure. The ambient pressure two-wire contact resistances for the samples were measured to be on the order of $R \sim 1\ \Omega$, which generally improved throughout the investigation to slightly less than 1 Ω as the pressure was increased from P = 0 to ∼2 GPa. An excitation current of less than 1 mA was applied for all measurements of electrical resistivity in this work. A 1:1 mixture by volume of *n*-pentane and isoamyl alcohol was used to provide a quasi-hydrostatic pressure transmitting medium and the pressure was locked in with the use of a beryllium copper clamped piston-cylinder pressure cell. The pressure dependence of the superconducting transition temperature of high-purity Sn was used as a manometer. Measurements of $\rho(T)$ were performed upon warming from ∼1 to 300 K in a pumped ^{4}He Dewar and the temperature was determined from a calibrated Cernox resistance thermometer.

Data Availability. All study data are included in this article and/or *SI Appendix*.

ACKNOWLEDGMENTS. Research at the University of California San Diego was supported by the US Department of Energy (DOE), Office of Basic Energy Sciences, Division of Materials Sciences and Engineering, under Grant DE-FG02-04ER46105 (materials synthesis and characterization); the US NSF under Grant DMR 1810310 (low-temperature measurements); and the National Nuclear Security Administration under the Stewardship Science Academic Alliance Program through the US DOE under Grant DE-NA0002909 (high-pressure measurements). Research at the National High Magnetic Field Laboratory was supported by NSF Cooperative Agreement DMR-1157490, the State of Florida, and the DOE.

1. T. T. M. Palstra *et al.*, Superconducting and magnetic transitions in the heavy-fermion system URu_2Si_2. *Phys. Rev. Lett.* **55**, 2727 (1985).
2. M. B. Maple *et al.*, Partially gapped Fermi surface in the heavy-electron superconductor URu_2Si_2. *Phys. Rev. Lett.* **56**, 185 (1986).
3. W. Schlabitz *et al.*, Superconductivity and magnetic order in a strongly interacting fermi-system: URu_2Si_2. *Z. Phys. B Condens. Matter* **62**, 171 (1986).
4. C. Broholm *et al.*, Magnetic excitations and ordering in the heavy-electron superconductor URu_2Si_2. *Phys. Rev. Lett.* **58**, 1467–1470 (1987).
5. J. Schoenes, C. Schönenberger, J. J. M. Franse, A. A. Menovsky, Hall-effect and resistivity study of the heavy-fermion system URu_2Si_2. *Phys. Rev. B* **35**, 5375–5378 (1987).
6. M. W. McElfresh *et al.*, Effect of pressure on competing electronic correlations in the heavy-electron system URu_2Si_2. *Phys. Rev. B* **35**, 43–47 (1987).
7. A. L. Dawson, W. R. Datars, J. D. Garrett, F. S. Razavi, Electrical transport in uru_2si_2. *J. Phys. Condens. Matter* **1**, 6817 (1989).
8. T. E. Mason, W. J. L. Buyers, Spin excitations and the electronic specific heat of URu_2Si_2. *Phys. Rev. B* **43**, 11471 (1991).
9. C. Broholm *et al.*, Magnetic excitations in the heavy-fermion superconductor URu_2Si_2. *Phys. Rev. B* **43**, 12809 (1991).
10. P. Santini, G. Amoretti, Crystal field model of the magnetic properties of URu_2Si_2. *Phys. Rev. Lett.* **73**, 1027 (1994).
11. W. J. L. Buyers *et al.*, Spin wave collapse and incommensurate fluctuations in URu_2Si_2. *Phys. B Condens. Matter* **199-200**, 95 (1994).
12. R. Escudero, F. Morales, P. Lejay, Temperature dependence of the antiferromagnetic state in URu_2Si_2 by point-contact spectroscopy. *Phys. Rev. B* **49**, 15271 (1994).
13. H. Amitsuka *et al.*, Effect of pressure on tiny antiferromagnetic moment in the heavy-electron compound URu_2Si_2. *Phys. Rev. Lett.* **83**, 5114–5117 (1999).
14. P. Chandra, P. Coleman, J. A. Mydosh, V. Tripathi, Hidden orbital order in the heavy fermion metal URu_2Si_2. *Nature* **417**, 831 (2002).
15. F. Bourdarot, B. Fåk, K Habicht, K. Prokeš, Inflection point in the magnetic field dependence of the ordered moment of URu_2Si_2 observed by neutron scattering in fields up to 17 T. *Phys. Rev. Lett.* **90**, 067203 (2003).
16. C. R. Wiebe, G. M. Luke, Z. Yamani, A. A. Menovsky, W. J. L. Buyers, Search for hidden orbital currents and observation of an activated ring of magnetic scattering in the heavy fermion superconductor URu_2Si_2. *Phys. Rev. B* **69**, 132418 (2004).
17. K. Behnia *et al.*, Thermal transport in the hidden-order state of URu_2Si_2. *Phys. Rev. Lett.* **94**, 156405 (2005).
18. J. R Jeffries, N. P. Butch, B. T. Yukich, M. B. Maple, Competing ordered phases in URu_2Si_2: Hydrostatic pressure and rhenium substitution. *Phys. Rev. Lett.* **99**, 217207 (2007).
19. C. R. Wiebe *et al.*, Gapped itinerant spin excitations account for missing entropy in the hidden-order state of URu_2Si_2. *Nat. Phys.* **3**, 96 (2007).
20. S. Elgazzar, J. Rusz, M. Amft, P. M. Oppeneer, J. A. Mydosh, Hidden order in URu_2Si_2 originates from Fermi surface gapping induced by dynamic symmetry breaking. *Nat. Mater.* **8**, 337 (2009).
21. J. A. Janik *et al.*, Itinerant spin excitations near the hidden order transition in URu_2Si_2. *J. Phys. Condens. Matter* **21**, 192202 (2009).
22. A. F. Santander-Syro *et al.*, Fermi-surface instability at the 'hidden-order' transition of URu_2Si_2. *Nat. Phys.* **5**, 637 (2009).
23. K. Haule, G. Kotliar, Complex Landau-Ginzburg theory of the hidden order in URu_2Si_2. *Europhys. Lett.* **89**, 57006 (2010).
24. R. Yoshida *et al.*, Signature of hidden order and evidence for periodicity modification in URu_2Si_2. *Phys. Rev. B* **82**, 205108 (2010).
25. A. R. Schmidt *et al.*, Imaging the Fano lattice to 'hidden order' transition in URu_2Si_2. *Nature* **465**, 570 (2010).
26. P. Aynajian *et al.*, Visualizing the formation of the Kondo lattice and the hidden order in URu_2Si_2. *Proc. Natl. Acad. Sci. U.S.A.* **107**, 10383 (2010).
27. P. M. Oppeneer *et al.*, Electronic structure theory of the hidden-order material URu_2Si_2. *Phys. Rev. B* **82**, 205103 (2010).

28. P. M. Oppeneer *et al.*, Spin and orbital hybridization at specifically nested Fermi surfaces in URu_2Si_2. *Phys. Rev. B* **84**, 241102 (2011).
29. I. Kawasaki *et al.*, Band structure and Fermi surface of URu_2Si_2 studied by soft x-ray angle-resolved photoemission spectroscopy. *Phys. Rev. B* **83**, 235121 (2011).
30. G. L. Dakovski *et al.*, Anomalous femtosecond quasiparticle dynamics of hidden order state in URu_2Si_2. *Phys. Rev. B* **84**, 161103 (2011).
31. Y. Dubi, A. V. Balatsky, Hybridization wave as the "hidden order" in URu_2Si_2. *Phys. Rev. Lett.* **106**, 086401 (2011).
32. J. T. Haraldsen, Y. Dubi, N. J. Curro, A. V. Balatsky, Hidden-order pseudogap in URu_2Si_2. *Phys. Rev. B* **84**, 214410 (2011).
33. C. Pépin, M. R. Norman, S. Burdin, A. Ferraz, Modulated spin liquid: A new paradigm for URu_2Si_2. *Phys. Rev. Lett.* **106**, 106601 (2011).
34. P. S. Riseborough, B. Coqblin, S. G. Magalhães, Phase transition arising from the underscreened Anderson lattice model: A candidate concept for explaining hidden order in URu_2Si_2. *Phys. Rev. B* **85**, 165116 (2012).
35. J. A. Mydosh, P. M. Oppeneer, Colloquium: Hidden order, superconductivity, and magnetism: The unsolved case of URu_2Si_2. *Rev. Mod. Phys.* **83**, 1301–1322 (2011).
36. J. Q. Meng *et al.*, Imaging the three-dimensional fermi-surface pairing near the hidden-order transition in URu_2Si_2 using angle-resolved photoemission spectroscopy. *Phys. Rev. Lett.* **111**, 127002 (2013).
37. F. L. Boariu *et al.*, Momentum-resolved evolution of the Kondo lattice into "hidden order" in URu_2Si_2. *Phys. Rev. Lett.* **110**, 156404 (2013).
38. C. Bareille *et al.*, Momentum-resolved hidden-order gap reveals symmetry breaking and origin of entropy loss in URu_2Si_2. *Nat. Commun.* **5**, 637 (2009).
39. J. A. Mydosh, P. M. Oppeneer, Hidden order behaviour in URu_2Si_2 (A critical review of the status of hidden order in 2014). *Philos. Mag.* **94**, 3642–3662 (2014).
40. N. P. Butch *et al.*, Symmetry and correlations underlying hidden order in URu_2Si_2. *Phys. Rev. B* **91**, 035128 (2015).
41. S. Ran *et al.*, Phase diagram and thermal expansion measurements on the system $URu_{2-x}Fe_xSi_2$. *Proc. Natl. Acad. Sci. U.S.A.* **113**, 13348 (2016).
42. H. H. Kung *et al.*, Analogy between the "hidden order" and the orbital antiferromagnetism in $URu_{2-x}Fe_xSi_2$. *Phys. Rev. Lett.* **117**, 227601 (2016).
43. S. Ran *et al.*, Phase diagram of $URu_{2-x}Fe_xSi_2$ in high magnetic fields. *Proc. Natl. Acad. Sci. U.S.A.* **114**, 9826–9831 (2017).
44. Y. Dalichaouch, M. B. Maple, M. S. Torikachvili, A. L. Giorgi, Ferromagnetic instability in the heavy-electron compound URu_2Si_2 doped with Re or Tc. *Phys. Rev. B* **39**, 2423 (1989).
45. Y. Dalichaouch *et al.*, Effect of transition-metal substitutions on competing electronic transitions in the heavy-electron compound URu_2Si_2. *Phys. Rev. B* **41**, 1829 (1990).
46. Y. Dalichaouch *et al.*, Ferromagnetism and heavy electron behavior in $URu_{2-x}M_xSi_2$ (M = Re, Tc and Mn). *Phys. B Condens. Matter* **163**, 113 (1990).
47. N. P. Butch, M. B. Maple, The suppression of hidden order and the onset of ferromagnetism in URu_2Si_2 via Re substitution. *J. Phys. Condens. Matter* **22**, 164204 (2010).
48. M. Yokoyama *et al.*, Neutron scattering study on competition between hidden order and antiferromagnetism in $U(Ru_{1-x}Rh_x)_2Si_2$ ($x \leq 0.05$). *J. Phys. Soc. Japan* **73**, 545 (2004).
49. A. Lopez de la Torre, P. Visani, Y. Dalichaouch, B. W. Lee, M. B. Maple, Th-doped URu_2Si_2: Influence of Kondo holes on coexisting superconductivity and magnetism. *Phys. B Condens. Matter* **179**, 208 (1992).
50. J. G. Park, B. R. Coles, Studies of alloying effects on URu_2 $(Si,X)_2$; X=Al or Ge. *J. Phys. Condens. Matter* **6**, 1425 (1994).
51. S. Zwirner *et al.*, Anisotropic magnetic coupling in $Np_xU_{1-x}Pd_2Al_3$, $Np_xU_{1-x}Ru_2Si_2$. *Phys. B Condens. Matter* **230-232**, 80 (1997).
52. A. Gallagher *et al.*, Unfolding the physics of URu_2Si_2 through silicon to phosphorus substitution. *Nat. Commun.* **7**, 10712 (2016).
53. N. P. Butch *et al.*, Antiferromagnetic critical pressure in URu_2Si_2 under hydrostatic conditions. *Phys. Rev. B* **82**, 060408 (2010).
54. J. R. Jeffries, N. P. Butch, B. T. Yukich, M. B. Maple, The evolution of the ordered states of single-crystal URu_2Si_2 under pressure. *J. Phys. Condens. Matter* **20**, 095225 (2008).
55. F. Bourdarot *et al.*, Pressure dependence of magnetic transitions in URu_2Si_2. *Physica B* **350**, E179–E181 (2004).
56. H. Amitsuka *et al.*, Pressure-temperature phase diagram of the heavy-electron superconductor URu_2Si_2. *J. Magn. Magn, Mater.* **310**, 214–220 (2007).
57. N. Kanchanavatee *et al.*, Twofold enhancement of the hidden-order/large-moment antiferromagnetic phase boundary in the $URu_{2-x}Fe_xSi_2$ system. *Phys. Rev. B* **84**, 245122 (2011).
58. P. Das *et al.*, Chemical pressure tuning of URu_2Si_2 via isoelectronic substitution of Ru with Fe. *Phys. Rev. B* **91**, 085122 (2015).
59. C. T. Wolowiec, N. Kanchanavatee, K. Huang, S. Ran, M. B. Maple, Evolution of critical pressure with increasing Fe substitution in the heavy-fermion system $URu_{2-x}Fe_xSi_2$. *Phys. Rev. B* **94**, 085145 (2016).
60. M. N. Wilson *et al.*, Antiferromagnetism and hidden order in isoelectronic doping of URu_2Si_2. *Phys. Rev. B* **93**, 064402 (2016).
61. N. Kanchanavatee, B. D. White, V. W. Burnett, M. B. Maple, Enhancement of the hidden order/large moment antiferromagnetic transition temperature in the $URu_{2-x}Os_xSi_2$ system. *Philos. Mag.* **94**, 3681 (2014).
62. J. S. Hall *et al.*, Electrodynamics of the antiferromagnetic phase in URu_2Si_2. *Phys. Rev. B* **92**, 195111 (2015).
63. J. Denlinger *et al.*, Comparative study of the electronic structure of XRu_2Si_2: Probing the Anderson lattice. *J. Electron. Spectrosc. Relat. Phenom.* **117-118**, 347 (2001).
64. S. Kambe *et al.*, Thermal expansion under uniaxial pressure in URu_2Si_2. *Phys. Rev. B* **87**, 115123 (2013).
65. M. B. Fontes *et al.*, Electron-magnon interaction in *R*NiBC (R = Er, Ho, Dy, Tb, and Gd) series of compounds based on magnetoresistance measurements. *Phys. Rev. B* **60**, 6781–6789 (1999).
66. K. Matsuda, Y. Kohori, T. Kohara, K. Kuwahara, H. Amitsuka, Spatially inhomogeneous development of antiferromagnetism in URu_2Si_2: Evidence from ^{29}Si NMR under pressure. *Phys. Rev. Lett.* **87**, 087203 (2001).
67. M. Nakashima *et al.*, The de Haas-van Alphen effect in URu_2Si_2 under pressure. *J. Phys. Condens. Matter* **15**, S2011 (2003).
68. A. Villaume *et al.*, Signature of hidden order in heavy fermion superconductor URu_2Si_2: Resonance at the wave vector $Q_0 = (1, 0, 0)$. *Phys. Rev. B* **78**, 012504 (2008).
69. P. G. Niklowitz *et al.*, Parasitic small-moment antiferromagnetism and nonlinear coupling of hidden order and antiferromagnetism in URu_2Si_2 observed by larmor diffraction. *Phys. Rev. Lett.* **104**, 106406 (2010).
70. F. Bourdarot *et al.*, Magnetic properties of URu_2Si_2 under uniaxial stress by neutron scattering. *Phys. Rev. B* **84**, 184430 (2011).
71. T. J. Williams *et al.*, Gapped excitations in the high-pressure antiferromagnetic phase of URu_2Si_2. *Phys. Rev. B* **95**, 195171 (2017).
72. S. Chatterjee *et al.*, Formation of the coherent heavy fermion liquid at the hidden order transition in URu_2Si_2. *Phys. Rev. Lett.* **110**, 186401 (2013).
73. N. P. Butch *et al.*, Distinct magnetic spectra in the hidden order and antiferromagnetic phases in $URu_{2-x}Fe_xSi_2$. *Phys. Rev. B* **94**, 201102 (2016).
74. H. Drickamer, The effect of high pressure on the electronic structure of solids. *Solid State Phys.* **17**, 1–133 (1965).
75. H. G. Drickamer, C. W. Frank, *Electronic Transitions and the High Pressure Chemistry and Physics of Solids (Studies in Chemical Physics,* Springer Netherlands, 1973).
76. J. S. Schilling, Pressure as a parameter in the study of dilute magnetic alloys. *Adv. Phys.* **28**, 657 (1979).
77. J. S. Schilling, "Some recent results in magnetism under high pressure" in *Physics of Solids Under High Pressure*, J. S. Schilling, R. S. Shelton, Eds. (North-Holland Publishing Company, Amsterdam, The Netherlands, 1981), pp. 345–356.
78. M. B. Maple, J. Wittig, K. S. Kim, Pressure-induced magnetic-nonmagnetic transition of Ce impurities in La. *Phys. Rev. Lett.* **23**, 1375 (1969).
79. K. S. Kim, M. B. Maple, Kondo effect in $La_{1-x}Ce_x$ alloys under pressure. *Phys. Rev. B* **2**, 4696 (1970).
80. M. B. Maple, Superconductivity - a probe of the magnetic state of local moments in metals. *Appl. Phys.* **9**, 179 (1976).
81. J. B. Mann, SCF Hartree-Fock results for elements with two open shells and the elements francium to nobelium. *Atomic Data Nucl. Data Tables* **12**, 1–86 (1973).
82. A. D. McLean, R. S. McLean, Roothaan-Hartree-Fock atomic wave functions Slater basis-set expansions for Z = 55-92. *Atomic Data Nucl. Data Tables* **26**, 197 (1981).
83. D. A. Papaconstantopoulos, M. J. Mehl, The Slater-Koster tight-binding method: A computationally efficient and accurate approach. *J. Phys. Condens. Matter* **15**, R413 (2003).
84. J. Durgavich, S. Sayed, D. Papaconstantopoulos, Extension of the NRL tight-binding method to include f orbitals and applications in Th, Ac, La and Yb. *Comput. Mater. Sci.* **112**, 395 (2016).
85. D. A. Papaconstantopoulos, *Handbook of the Band Structure of Elemental Solids* (Springer US, New York, NY, ed. 2, 2015).
86. L. P. Regnault, W. A. C. Erkelens, J. Rossat-Mignod, P. Lejay, J. Flouquet, Neutron scattering study of the heavy-fermion compound $CeRu_2Si_2$. *Phys. Rev. B* **38**, 4481 (1988).
87. M. Koterlyn, I. Shcherba, R. Yasnitskii, G. Koterlyn, Peculiarities of the intermediate valence state of Ce in CeM_2Si_2 (*M*=Fe, Co, Ni) compounds. *J. Alloys Compd.* **442**, 176 (2007).
88. M. Besnus, J. Kappler, P. Lehmann, A. Meyer, Low temperature heat capacity, magnetization, resistivity of $CeRu_2Si_2$, with Y or La substitution. *Solid State Commun.* **55**, 779 (1985).
89. A. Umarji, G. Claude, L. Gupta, R. Vijayaraghavan, Spin fluctuation effects in substituted $CeRu_2Si_2$ and $YbPd_2Si_2$ alloys. *Pramana* **27**, 321 (1986).
90. Y. Kitaoka *et al.*, NMR investigation of superconductivity and kondo-coherency in $CeCu_2Si_2$. *J. Phys. Soc. Jpn.* **55**, 723 (1986).
91. C. Godart, A. M. Umarji, L. C. Gupta, R. Vijayaraghavan, Magnetism and spin fluctuation effects in heavy-fermion $CeRu_2Si_2$ induced by partial substitution of Ru and Si. *Phys. Rev. B* **34**, 7733 (1986).
92. A. Amorese *et al.*, From antiferromagnetic and hidden order to Pauli paramagnetism in UM_2Si_2 compounds with 5*f* electron duality. *Proc. Natl. Acad. Sci.* U.S.A. **117**, 30220–30227 (2020).
93. Y. S. Oh *et al.*, Interplay between Fermi surface topology and ordering in URu_2Si_2 revealed through abrupt Hall coefficient changes in strong magnetic fields. *Phys. Rev. Lett.* **98**, 016401 (2007).
94. Y. J. Jo *et al.*, Field-induced Fermi surface reconstruction and adiabatic continuity between antiferromagnetism and the hidden-order state in URu_2Si_2. *Phys. Rev. Lett.* **98**, 166404 (2007).
95. B. H. Toby, R. B. Von Dreele, *GSAS-II*: The genesis of a modern open-source all purpose crystallography software package. *J. Appl. Crystallogr.* **46**, 544 (2013).